Journal of Materials and Environmental Science
ISSN : 2028-2508
e-ISSN : 2737-890X
CODEN : JMESCN

J. Mater. Environ. Sci., 2024, Volume 15, Issue 7, Page 934-954

http://www.jmaterenvironsci.com

Photocatalytic Degradation of Methyl Orange (MO) and Sulfamethoxazole (SMX) by Superparamagnetic Magnetite (Fe_3O_4) Nanoparticles

Md. Abdus Sabur[1*], Md. Abdul Gafur[1], Md. Newaz Sharif[2]

[1]*Pilot Plant and Process Development Centre, Bangladesh Council of Scientific and Industrial Research (BCSIR), Dhanmondi, Dhaka-1205, Bangladesh*

[2]*Department of Chemistry, Jahangirnagar University, Savar, Dhaka-1342, Bangladesh*

**Corresponding author, Email address: sabur37971@gmail.com*

Received *29 Mar 2024,*
Revised *07 July 2024,*
Accepted *09 July 2024*

Keywords:
- ✓ *Magnetite nanoparticles;*
- ✓ *Co-precipitation;*
- ✓ *Photocatalysis;*
- ✓ *Methyl orange;*
- ✓ *Sulfamethoxazole;*
- ✓ *Antibiotics*

Citation*: Sabur M. A., Gafur M. A., Sharif M. N. (2024) Photocatalytic Degradation of Methyl Orange (MO) and Sulfamethoxazole (SMX) by Superparamagnetic Magnetite (Fe_3O_4) Nanoparticles, J. Mater. Environ. Sci., 15(7), 934-954.*

Abstract: Magnetite nanoparticles (Fe_3O_4) were synthesized by chemical co-precipitation method using ferric chloride and heptahydrate ferrous sulfate salts utilizing sodium hydroxide as a precipitant. The produced powders were analyzed using an X-ray diffractometer, Fourier-transform infrared spectrometer, transmission electron microscope, scanning electron microscope, and atomic force microscope to ascertain the size, shape, and chemical composition of the manufactured magnetite nanoparticles. It was found that the magnetite powder had formed spherical-like particles with diameters of roughly 30 nm and a face-centered cubic crystal structure. A vibrating sample magnetometer was used to assess the magnetic characteristics of magnetite nanoparticles. The obtained superparamagnetic properties of the produced nanoparticles, with saturation magnetization and coercivity of 50.75 emu/g and 30.09 Oe, respectively allow them for the degradation of antibiotics, and removal of organic dyes. Further study of photocatalytic degradation of methyl orange using Fe_3O_4 nanoparticles was done. Fe_3O_4 nanoparticles demonstrated possible catalytic activity by reducing methyl orange by 75.39%. Additionally, the photocatalytic activity of Fe_3O_4 nanoparticles was analyzed against sulfamethoxazole antibiotic where Fe_3O_4 nanoparticles degraded sulfamethoxazole antibiotic by 24.73%.

1. Introduction

Due to the necessity for dyes to change the color of cloth and antibiotics for human treatment, industries like the pharmaceutical and textile industries have had to grow as a result of the increase in the global human population (Ahmed *et al.,* 2015). As a result, there is now more demand, which has increased production and usage. Water contamination in the environment has been caused by the inappropriate disposal and direct discharge of dyes and pharmaceutical pollutants from the textile industry and hospital effluents (Al-Hakkani *et al.,* 2021; Rais *et al.* 2008). These effluents contain toxins that enter water

bodies and degrade the ecosystem globally, rendering drinking water unsafe for consumption (Akinola *et al.,* 2020; Anchan *et al.,* 2019). Water is the basis of life, and exposure to these chemicals harms the ecosystem, endangering the health of both humans and animals (Shaker Ardakani *et al.,* 2021). The central nervous system, the gastrointestinal tract, and the respiratory system have all been known to be harmed by organic dyes (Bahadur *et al.,* 2017). Additionally, the increased use of antibiotics may have permanent and long-lasting consequences on microbes by promoting genetic exchange, which would subsequently hasten the development of antibiotic-resistant (bacteria species) pathogens (Bahadur *et al.,* 2017). When illnesses, syndromes, and diseases occur as a result, this promotes human health concerns (Bhuiyan *et al.,* 2020; Bibi *et al.,* 2019).

Several methods such as floatation, ion exchange, chlorination, adsorption, and electrochemical methods have been used for the removal of dyes, bacteria, and pharmaceutical drugs in water in particular pollutants such as methylene blue (MB), methyl orange (MO) malachite green (MG), E. coli, Amoxicillin, Diclofenac, S. aureus, ciprofloxacin, sulfamethoxazole (SMX) and sulfisoxazole (SSX) respectively (Anchan *et al.,* 2019; Bahadur *et al.,* 2017). Most of these techniques are expensive, call for delicate equipment, and produce items that cannot be recycled (Bhuiyan *et al.,* 2020; Bibi *et al.,* 2019). All samples must be pre-treated for ion exchange, and standardization is necessary for biological procedures even though these techniques are typically ineffective. Researchers choose photocatalysis over the other approaches because it has been demonstrated to destroy complex pollutants, is simple to apply, and can yield repeatable results (Devi *et al.,* 2019; González-González *et al.,* 2022).

Metal oxides have been employed as photocatalysts for the degradation of several contaminants from wastewater, including Zinc Oxide, Iron Oxide, Titanium dioxide, and Nickel Oxide (Juárez-Rojop *et al.,* 2014; Kiwumulo *et al.,* 2022; Akinola *et al.,* 2020). Due to their superparamagnetic characteristics and biocompatibility, Fe_3O_4 nanoparticles are useful as contrast agents in MRIs (Rezayan *et al.,* 2016), drug delivery systems (Thu Huong *et al.,* 2016), catalysts (Arefi *et al.,* 2015), antibacterial agents (Prabhu *et al.,* 2015), heavy metals absorbers (Kalantari *et al.,* 2014), and for capturing thermal energy from the sun directly (Chen *et al.,* 2016). Additionally, nanocomposites containing Fe_3O_4 nanoparticles can be employed as electromagnetic interference (EMI) shielding materials (Jian *et al.,* 2016) and electrochemical biosensors (Sanaeifar *et al.,* 2017).

Currently, a wide range of synthesis techniques for Fe_3O_4 nanoparticles have been presented. Additionally, their impact on the physicochemical characteristics, size, and form of Fe_3O_4 nanoparticles was studied. The co-precipitation approach, hydrothermal method, thermal decomposition (Wu *et al.,* 2011; Azzaoui *et al.,* 2023; Azzaoui *et al.*, 2024), polyol process (Abbas *et al.,* 2013), and high-temperature organic phase decomposition are the most used techniques for synthesis. In the latter, the metal-oleate complex can produce monodisperse nanoparticles (Hufschmid *et al.,* 2015; Aaddouz *et al.,* 2023).

Small Fe_3O_4 nanoparticles can be produced using the co-precipitation method from simple chemicals like $FeCl_3$, $FeCl_2$, or $FeSO_4$. Higher yield, high product purity, the lack of necessity to use organic solvents, easily reproducible, and low cost are some of the common advantages of this method (Lima-Tenório *et al.,* 2015; Wu *et al.,* 2016). However, the properties of the produced particles, such as size, shape, and composition are highly dependent on the reaction parameters such as temperature, pH, ionic

strength, nature of basic solution, and so on. According to the following reaction, Fe^{2+} and Fe^{3+} ions react with OH^- to form Fe_3O_4 nanoparticles (Ganapathe *et al.,* 2020):

$$Fe^{2+} + 2Fe^{3+} + 8OH^- \rightarrow Fe_3O_4 + 4H_2O$$

In this study, Fe_3O_4 nanoparticles were synthesized using sodium hydroxide (NaOH) as a precipitating agent together with ferric and ferrous salts. The nanoparticles were then analyzed using X-ray diffractometer (XRD), Fourier-transform infrared spectrometer (FTIR), scanning electron microscope (SEM), transmission electron microscope (TEM), atomic force microscope (AFM), vibrating sample magnetometer (VSM), and thermogravimetric and differential thermal analyzer (TG-DTA) to study the structural, morphological, magnetic, and thermal properties of superparamagnetic magnetite nanoparticles. The obtained nanoparticles showed promising properties to use in photocatalysis. This study showed that methyl orange (MO) dye as well as sulfamethoxazole (SMX) antibiotic was degraded utilizing Fe_3O_4 nanoparticles, and their photocatalytic behavior was studied using a UV-VIS spectrophotometer (UV-VIS).

2. Experimental Details

2.1. Materials

All chemical reagents used in the synthesis were of analytical quality, no further purification was necessary. Ferrous sulfate heptahydrate ($FeSO_4 \cdot 7H_2O$), sodium hydroxide (NaOH), and anhydrous ferric chloride ($FeCl_3$) with a purity of ≥ 98% were acquired from Merck (India).

2.2. Synthesis of Magnetite Nanoparticles

Figure 1 shows the overall process of synthesizing magnetite nanoparticles. Fe_3O_4 nanoparticles were synthesized by mixing 100 mL of 0.4M $FeCl_3$ with 100 mL of 0.2M $FeSO_4 \cdot 7H_2O$ as a precursor using the co-precipitation method. The reaction between the $FeCl_3$ solution and the $FeSO_4$ solution produces the ions Fe^{3+} and Fe^{2+}. A 3M solution of NaOH was gradually added drop by drop to the salt solutions as a precipitating agent. The mixture was heated to 80 °C for 60 minutes while being constantly agitated until the pH reached 12. Then, coal-black Fe_3O_4 particles are produced as a precipitate by reacting Fe^{3+} and Fe^{2+} with NaOH solution in a molar ratio of 2:1 with the aid of a magnetic stirrer hot plate. To obtain the pure Fe_3O_4 nanoparticles, the material was then repeatedly washed in distilled water until its pH level reached 7. Lastly, the particles were calcined at 250°C for 4 hours.

2.3. Methods

2.3.1. Photocatalytic Degradation of Methyl Orange using Fe_3O_4 Nanoparticles

Following a procedure previously described by numerous publications (Hufschmid *et al.,* 2015; Mahlaule-Glory *et al.,* 2022) the photocatalytic degradation of organic dyes using Fe_3O_4 nanoparticles was examined using a UV light. In these degradation tests, 100 ml of the 5 ppm MO solution was mixed with 25 mg of the Fe_3O_4 photocatalyst in a 250 ml beaker, and kept the solution in an ultrasonic bath for 30 minutes. An adsorption-desorption experiment was conducted in the dark for around 30 minutes to

reach equilibrium before the light shone on the solution. The solution was then left under the UV lamp for 60 minutes. 5 ml of the solutions were taken and centrifuged at 10000 rpm for 5 minutes. The solution was then examined with a UV-VIS spectrometer at intervals of 15 minutes. The % of degradation was determined as follows:

$$\%\ of\ Degradation = \frac{(A_0 - A_t)}{A_0} \times 100$$

where A_0 indicates the initial absorption of the dye solution and A_t indicates the final absorption of the dye at specified time intervals.

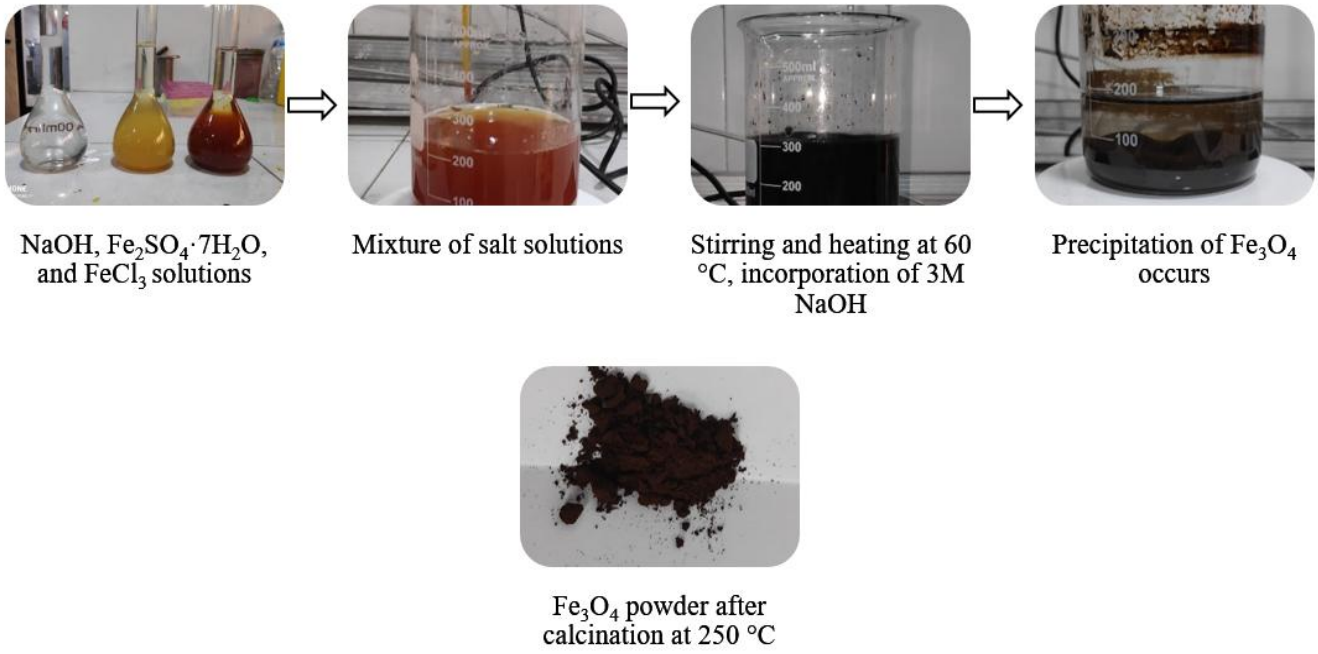

Figure 1. Synthesis of Fe_3O_4 nanoparticles by chemical co-precipitation method

2.3.2. Photocatalytic Degradation of Sulfamethoxazole using Fe_3O_4 Nanoparticles

A UV lamp was used to perform the photocatalytic degradation of the antibiotic. 50 mg of Fe_3O_4 nanoparticles were added to a 100 mL solution of 10 ppm of SMX antibiotic and kept the solution in an ultrasonic bath for 30 minutes. The solution was kept for 30 minutes in the dark before being exposed to radiation to establish an adsorption-desorption equilibrium. The mixture was then irradiated with UV light for 120 minutes. About 5 ml of the antibiotic solution was taken at intervals of 30 min, and the rate of degradation was measured by using a UV-VIS spectrometer.

The % of degradation was determined as follows:

$$\%\ of\ Degradation = \frac{(A_0 - A_t)}{A_0} \times 100$$

where A_0 indicates the initial absorption of the antibiotic solution and A_t indicates the final absorption of the antibiotic at specified time intervals.

2.4. Characterization Techniques

2.4.1. XRD

The crystallographic properties of Fe_3O_4 were identified by recording X-ray powder diffraction patterns (XRD) of powder samples using a Rigaku Smart Lab SE X-ray Diffractometer equipped with a CuKα radiation source (λ = 1.5406 Å). The analysis was done at 40 kV and 50 mA. The 2θ measured range was 20°–70° at 0.01° increments and 25.00°/min scan speed.

2.4.2. FTIR

To confirm the presence of different functional groups, FTIR spectra of Fe_3O_4 nanoparticles were recorded on a PerkinElmer SPECTRUM TWO FTIR Spectrometer within 450-4000 cm^{-1} region.

2.4.3. SEM

The morphology of Fe_3O_4 nanoparticles was observed using the JEOLUSER 7610F SEM, which operated at 10 kV. SEM images were analyzed with ImageJ software to calculate the particle size distribution of the dried nanoparticles.

2.4.4. TEM

The morphology of the Fe_3O_4 nanoparticles was analyzed by TEM using a High-Resolution LIBRA 120 Plus Carl Zeiss microscope. TEM images were analyzed with ImageJ software to calculate the particle size distribution of the dried nanoparticles.

2.4.5. AFM

AFM images were performed by CSI AFM Nano-observer microscopy in an oscillating mode using silicon cantilevers with a typical resonant frequency of 138.228 kHz, scanning speed of 750 mIn/s, resolution of 512×512, and scan size of 5μm×5μm. The AFM data were analyzed using the Gwyddion software.

2.4.6. VSM

The magnetic properties of Fe_3O_4 nanoparticles were measured using VSM in the quantum design physical property measurement system DYNACOOL at room temperature with a magnetic field in the range of -15000 to 15000 Oe. About 12.3 mg of dried samples were used for these measurements.

2.4.7. TG/DTA

The thermogravimetric and differential thermal analysis TG/DTA curves of Fe_3O_4 nanoparticles were obtained from EXSTAR 6000, TG/DTA 6300 thermal analyzer with a heating rate of 20 ºC/min. The mass of the solid specimen was about 15.032 mg and the whole measurements were carried out in a nitrogen atmosphere.

2.4.8. UV-VIS

The absorbance and photocatalytic degradation of MO and SMX were measured at room temperature using SHIMADZU UV-VIS 1901 spectrophotometer within the range of 190-1100 nm.

3. Result and Discussion

3.1. XRD Analysis

Figure 2 displays the XRD pattern of Fe_3O_4 nanoparticles. The crystal structure, lattice parameter, crystallite size, and crystal defects of Fe_3O_4 nanoparticles are all determined by this pattern. The most intense peak in the XRD patterns can be found at 2θ = 35.65º, which corresponds to the (311) plane of Fe_3O_4 nanoparticles. Strong peaks at 2θ = 30.25, 35.65, 36.37, 43.15, and 62.78 are observed in Fe_3O_4 nanoparticles, which validates the presence of magnetite diffraction planes at 220, 311, 222, 400, and 440, respectively. These peaks are characteristic of magnetite because of their crystalline structure and cubic shape. Consequently, the Fe_3O_4 nanoparticle diffractogram satisfies the requirements of the magnetite standard JCPDS 65-3107 (Andrade *et al.*, 2019; Fernandes *et al.*, 2013). The lattice parameter of the cubic crystal system is determined using the given formula.

$$a^2 = \frac{h^2 + k^2 + l^2}{d^2}$$

where a is the lattice parameter, h, k, and l are the Miller indices and d is the interplanar spacing. The calculated average lattice parameter of Fe_3O_4 nanoparticles is 8.398 Å (**Table 1**).

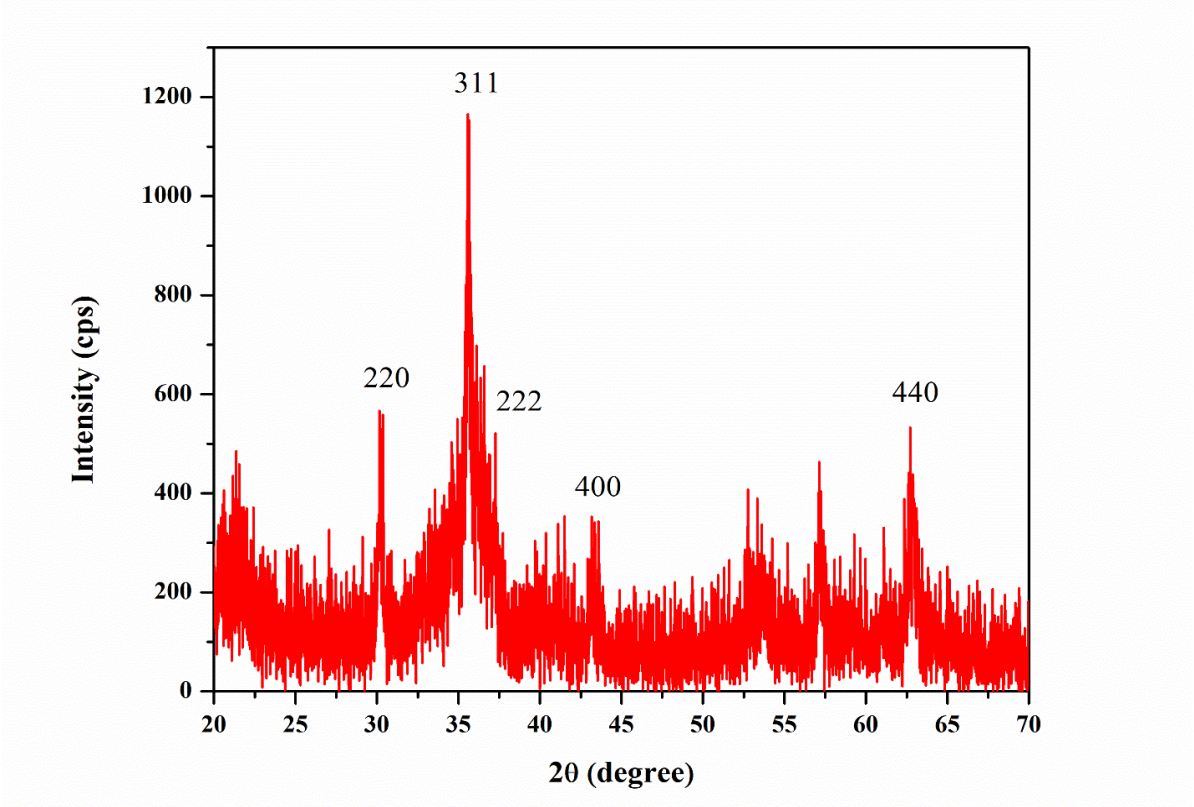

Figure 2. XRD pattern of Fe_3O_4 nanoparticles

The crystallite size is calculated using Debye-Scherrer's formula given below:

$$D = \frac{K\lambda}{\beta cos\theta}$$

where D is the average size of the crystallite, λ is the wavelength of X-ray radiation, β is the full peak width at half-maximum (FWHM) and θ is the angle of diffraction. The average crystallite size of Fe_3O_4 nanoparticles is 17.698 nm, and 34.862 nm for the most intense peak (**Table 1**).

The number of dislocations in a unit volume of crystalline materials is determined according to the Segal method as follows-

$$\delta = \frac{1}{D^2}$$

where δ is the dislocation density, and D is the crystallite size. The calculated average dislocation density of Fe_3O_4 nanoparticles is 3.219×10^{16} line/m^2 (**Table 1**).

The micro-strain of a crystalline solid is calculated using the following formula-

$$\epsilon = \frac{\beta}{4tan\theta}$$

ϵ is the micro-strain of the crystal, β is the full peak width at half-maximum (FWHM) and θ is the angle of diffraction. The average micro-strain of Fe_3O_4 nanoparticles is 0.0133 ppm (**Table 1**).

The magnetic properties of Fe_3O_4 nanoparticles, such as the Ms, Mr, and Hc, are significantly influenced by their crystallite size. Up to the critical limit, the Ms, Mr, and Hc increase with increasing crystallite size, regardless of the shape and crystal structure of the particles (Li *et al.,* 2017). The XRD measurements indicated that the Fe_3O_4 nanoparticles are superparamagnetic and had smaller Ms and Hc because of their smaller crystallite size.

Table 1. Crystallographic properties of Fe_3O_4 nanoparticles

S.N.	2θ (°)	h k l	d (Å)	Lattice parameter (Å)	Crystallite size (nm)	Dislocation density (line/m^2)	Micro-strain (ppm)
01	30.25	220	2.952	8.349	19.534	2.620×10^{15}	0.0071
02	35.65	311	2.516	8.344	34.862	8.227×10^{14}	0.0033
03	36.37	222	2.468	8.549	2.599	1.480×10^{17}	0.0446
04	43.15	400	2.095	8.380	12.057	6.878×10^{15}	0.0081
05	62.78	440	1.479	8.366	19.439	2.646×10^{15}	0.0035
Average				8.398	17.698	3.219×10^{16}	0.0133

3.2. FTIR Analysis

The FTIR spectrum of Fe_3O_4 nanoparticles is displayed in **Figure 3**. The band at 3390 cm^{-1} with 94 % transmittance for Fe_3O_4 nanoparticles corresponds to the H-O-H bond stretching mode of the absorbed or unbound water. In the crystalline lattice of Fe_3O_4, the stretching vibration mode linked to the metal-oxygen Fe-O bonds is responsible for the sharp peak that can be seen at 548 cm^{-1} with 68.73% transmittance. For ferrites in particular, they are notably prominent for all spinel configurations (Bordbar *et al.,* 2014; Jandl & Deslandes, 1981). The presence of hydroxyl groups is associated with a band at 1633 cm^{-1}.

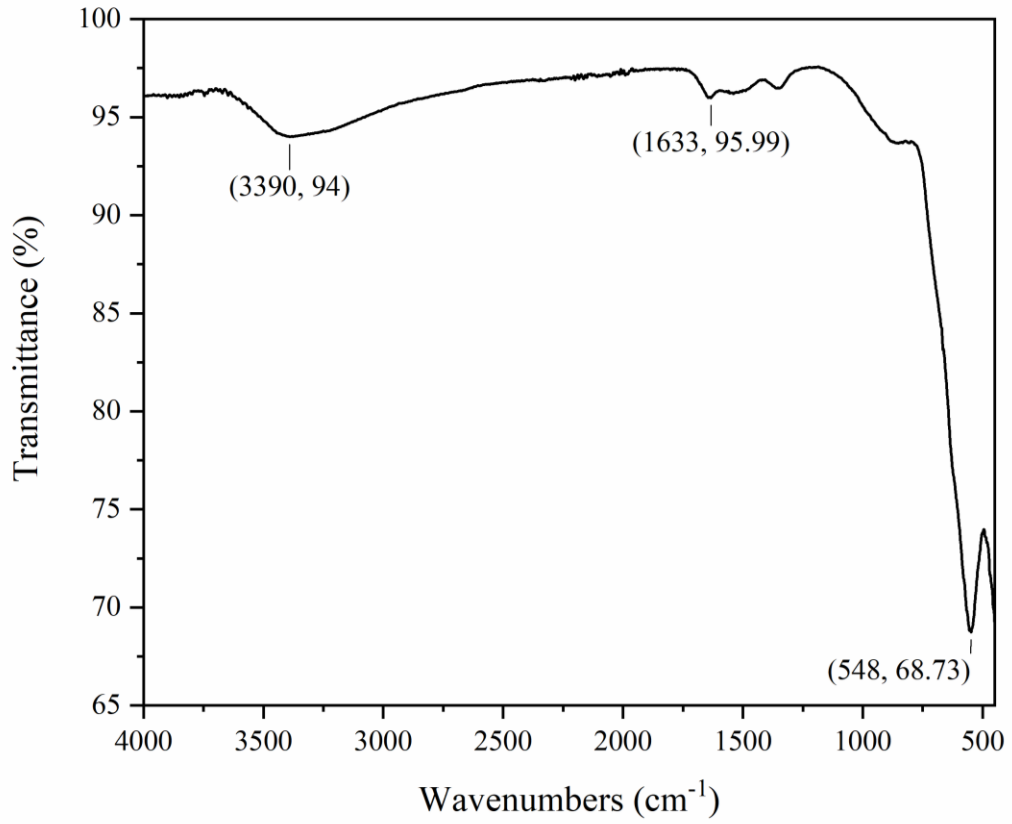

Figure 3. FTIR spectrum of Fe_3O_4 nanoparticles

3.3. SEM/EDAX Analysis

The average size, shape, and surface detail of the produced Fe_3O_4 nanoparticles are examined using SEM imaging. An FESEM image of Fe_3O_4 nanoparticles is shown in **Figure 4(a)**. The SEM image of the Fe_3O_4 nanoparticles illustrates that they have a rough surface and a spherical shape. Fe_3O_4 nanoparticles have an average particle size of 63 nm, as estimated by Image-J software (Alterary & Alkhamees, 2021). The size distribution of the nanoparticles is shown by the histogram (**Figure 4(b)**), and the average diameter of the produced nanoparticles is found to be 63.19 ± 7.12 nm. The EDAX spectrum of Fe_3O_4 nanoparticles reveals the presence of iron and oxygen (**Figure 4(c)**).

3.4.TEM Analysis

The size, shape, and morphology of the Fe_3O_4 nanoparticles are ascertained by taking TEM images. The HR-TEM image of Fe_3O_4 nanoparticles that underwent a 250 °C calcination is presented in **Figure 5(a)**. Using Image-J software, the HR-TEM image (**Figure 5(b)**) shows minute aggregated particles with a mean diameter of roughly 30 nm (Alterary & Alkhamees, 2021). The size distribution of the nanoparticles is shown by the histogram (**Figure 5(c)**), and the average diameter of the generated nanoparticles is found to be 29.56 ± 7.9 nm. The size distribution of the majority of the nanoparticles is between 25 and 35 nm. The existence of concentric rings connecting to multiple diffraction planes in

the selective area electron diffraction (SAED) pattern of the Fe_3O_4 nanoparticles indicates that the particles are polycrystalline (**Figure 5(d)**).

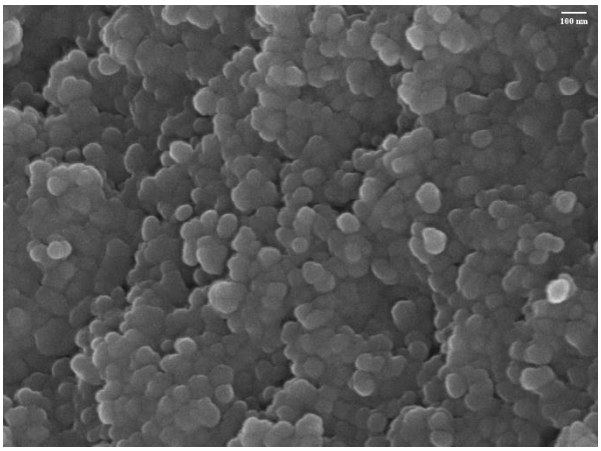

a)

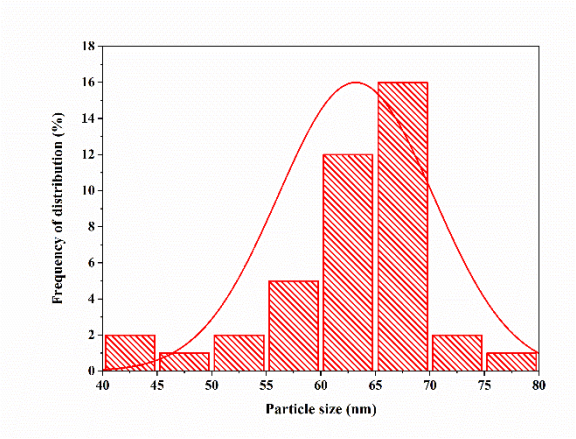

b)

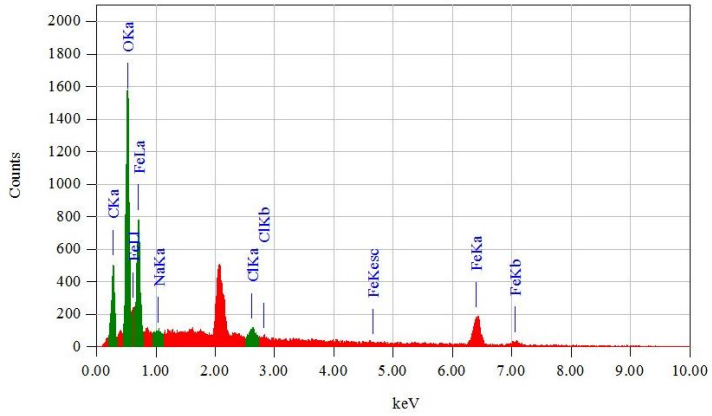

c)

Figure 4. a) FESEM image of Fe_3O_4 nanoparticles **b)** Size distribution of Fe_3O_4 nanoparticles **c)** EDAX image of Fe_3O_4 nanoparticles

3.5. AFM Analysis

AFM is used to assess the average size and shape of Fe_3O_4 nanoparticles. One or two droplets of 0.1 mg/mL nanoparticles were placed on a mica surface and allowed to dry at room temperature before the microscopy examinations. The Gwyddion software (Predoi *et al.*, 2021) is used to obtain and evaluate topography, amplitude, and phase contrast pictures from various places over the sample surface. A few typical micrographs are displayed in **Figures 6(a)**, **6(b)**, and **6(c)**, respectively. AFM pictures of magnetic nanoparticles typically show that the particles are made of a single phase of Fe_3O_4 and have an average diameter of 51.93 nm, giving them a virtually spherical shape. **Table 2** displays the particle size and surface roughness of Fe_3O_4 nanoparticles.

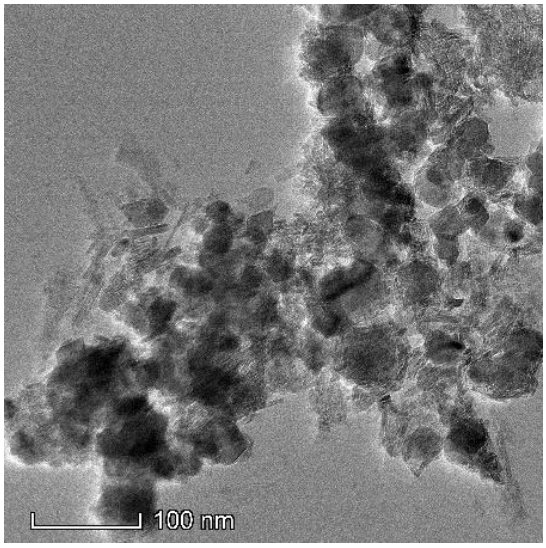

a)

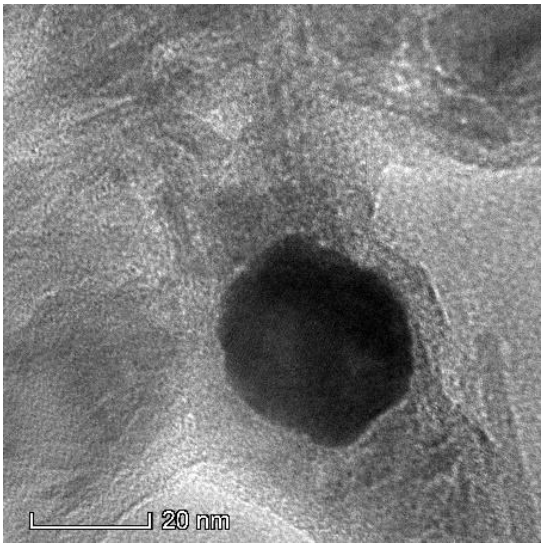

b)

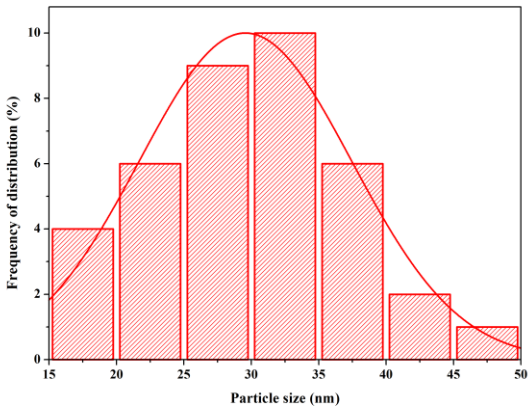

c)

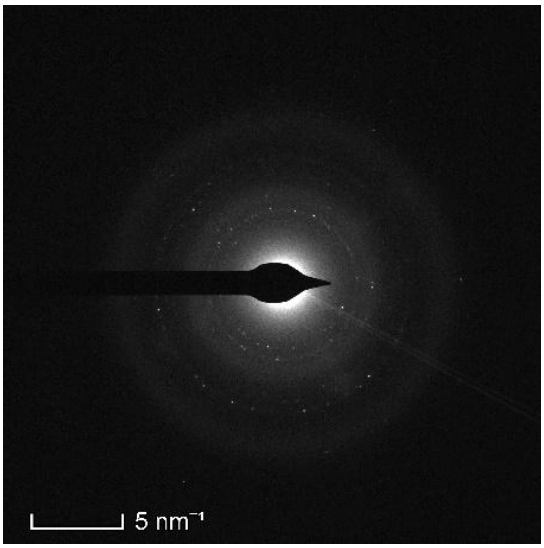

d)

Figure 5. a) TEM image of Fe_3O_4 nanoparticles **b)** HRTEM image of Fe_3O_4 nanoparticles **c)** Size distribution of Fe_3O_4 nanoparticles **d)** SAED pattern of Fe_3O_4 nanoparticles

3.6. VSM Analysis

Using a VSM, the magnetic properties of Fe_3O_4 nanoparticles are assessed. The hysteresis loops of Fe_3O_4 nanoparticles at room temperature are displayed in **Figure 7**, and **Table 3** provides a list of the magnetic characteristic values. The magnetization curve for the produced magnetite nanoparticles reported in this work shows very little hysteresis behavior for the samples and minimal values of remnant magnetization and coercivity field. This indicates that the generated particles exhibit superparamagnetic properties at room temperature. This is because magnetite nanoparticles that display superparamagnetic properties are smaller than the crucial size of the magnetic domain size (Goya *et al.,* 2003; Mahmed *et al.,* 2011; Wang *et al.,* 2013).

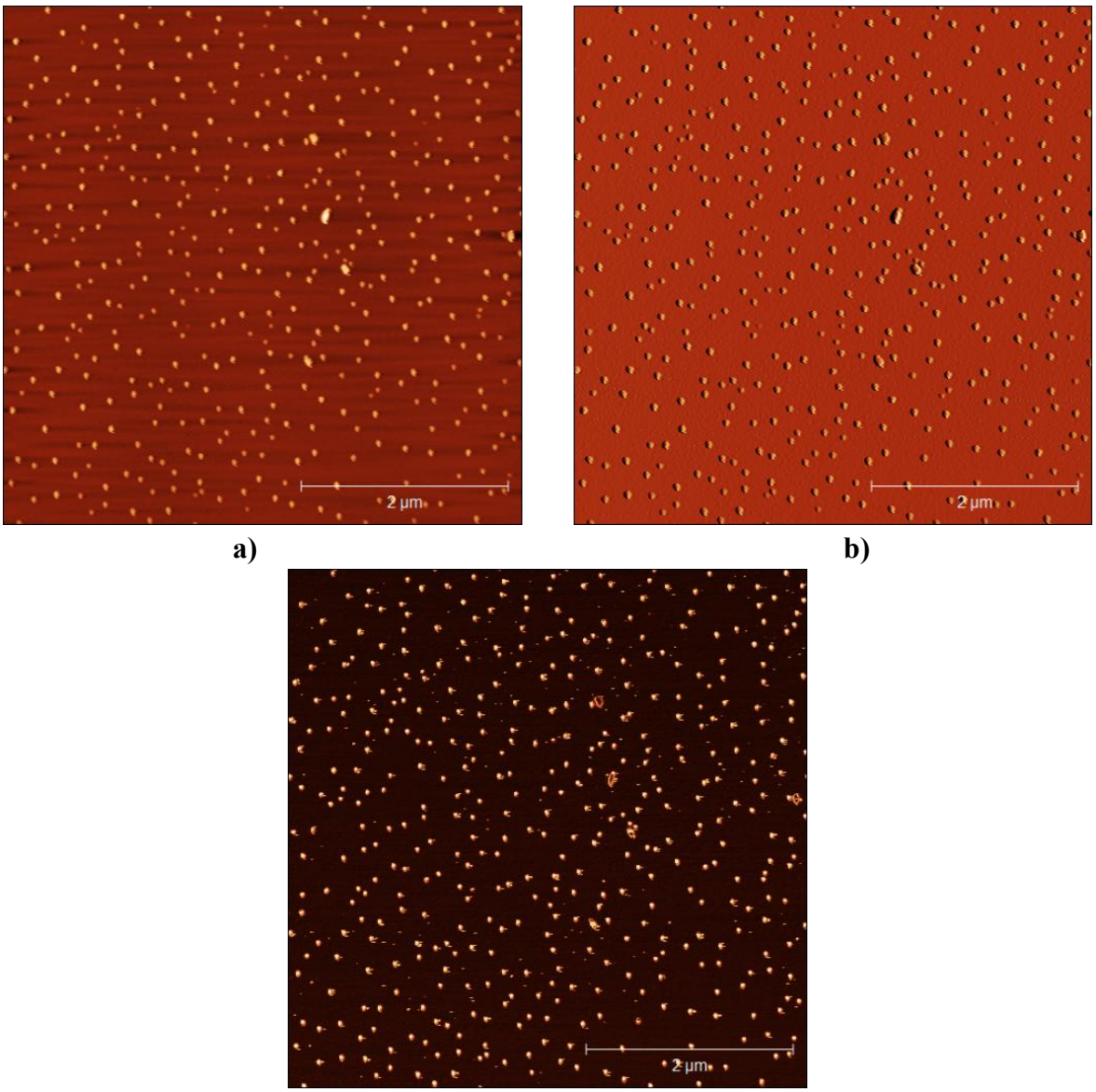

a) b)

c)

Figure 6. AFM image of Fe_3O_4 nanoparticles **a)** topography of Fe_3O_4 nanoparticles **b)** amplitude of Fe_3O_4 nanoparticles **c)** phase of Fe_3O_4 nanoparticles

Table 2. Particles size, and surface roughness of Fe_3O_4 nanoparticles

Average particle size (nm)	RMS roughness (nm)	Grain-wise RMS (nm)	Mean roughness (nm)
58.043	20.6954	20.6954	11.4536

In comparison to the bulk magnetite value of 92 emu/g, the superparamagnetism and saturation magnetization (Ms) values in the nanosized magnetite samples are lower (Schwertmann, 2003). Fe_3O_4

nanoparticles have saturation magnetization values of 50.75 emu/g. There are multiple explanations for why saturation magnetization decreases with smaller magnetite particle sizes. One aspect is related to the spin disorder layer, which increases with decreasing crystallite size. Another explanation for the decrease in the magnetic moment is the result of a dipolar interaction between magnetite nanoparticles. The value of saturation magnetization as a contribution from surface anisotropy may be impacted by the irregular form of magnetite particles. The manufactured samples are nearly spherical; thus surface anisotropy shouldn't have much of an impact. There can be a further decline in Ms if magnetite doesn't crystallize sufficiently during reaction synthesis. Saturation magnetization may be declining due to changes in the A and B site populations (Bødker *et al.,* 1994; Goya, 2002; Morales *et al.,* 1999). **Figure 7** illustrates the lack of a long-range magnetic dipole-dipole interaction between the assemblies of superparamagnetic nanoparticles by showing that hysteresis disappears at a tiny retentivity of 3.03 emu/g and coercivity (Hc) of 30.09 Oe. This suggests that the generated magnetite showed magnetization very fast upon being subjected to a magnetic field.

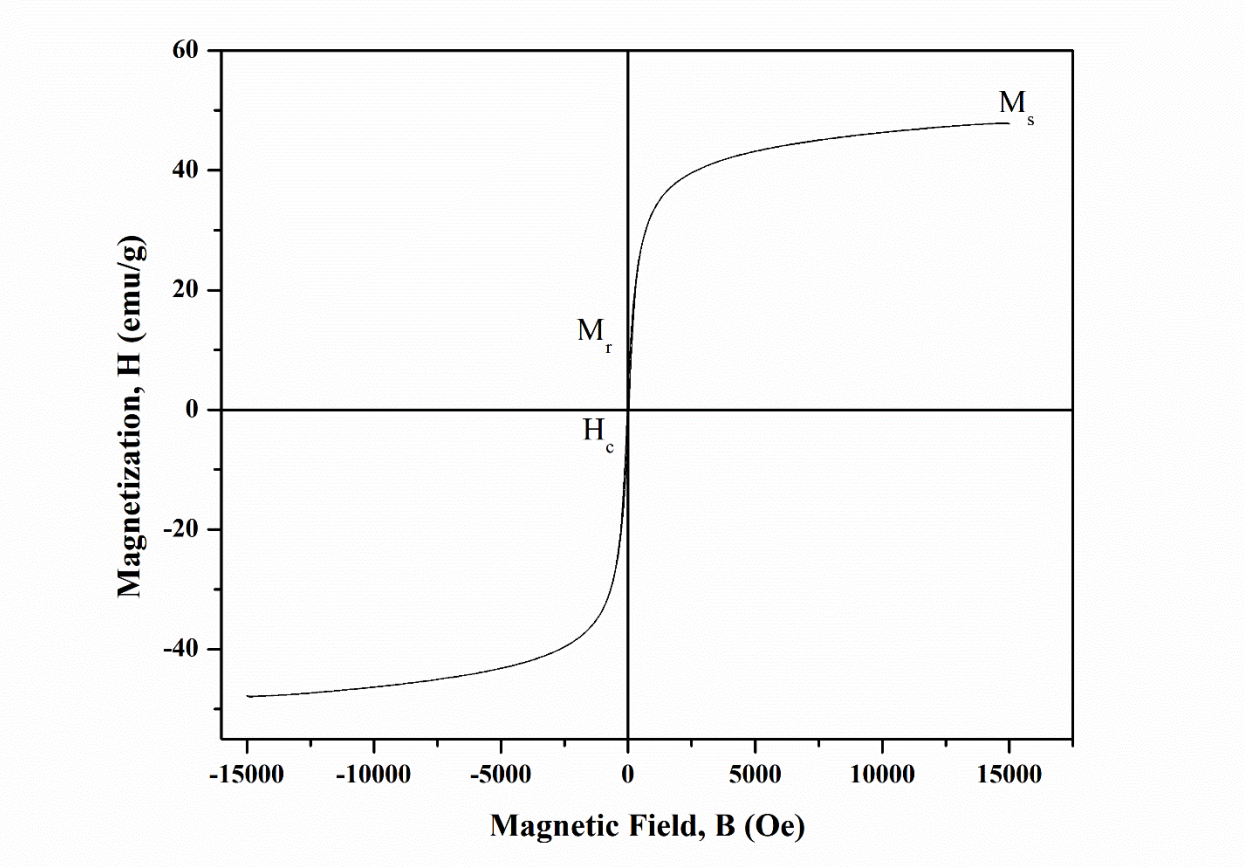

Figure 7. B-H (hysteresis) curve of Fe_3O_4 nanoparticles

Table 3. Magnetic properties of Fe_3O_4 nanoparticles

Saturation magnetization, emu/g	Remnant magnetization, emu/g	Coercivity, Oe
50.75	3.03	30.09

3.7. TG-DTA Analysis

Synchronized TG-DTA was performed on the Fe_3O_4 nanoparticles in a nitrogen environment at temperatures between 25 °C and 1000 °C, with a 20 °C/min increment. The TG graph (**Figure 8**) shows that three consistent weight losses have been found. The evaporation of absorbed water results in a significant weight loss of approximately 9.2% at temperatures between 30 and 180 °C. The second weight loss happens between 180 and 625 °C and is brought on by the breakdown of unrefined material like NaOH. The spinel phase and corresponding metal oxide production are confirmed by the third weight loss. Above 625 °C, there is no weight loss; instead, TGA curves stay stable, indicating the absolute volatility of water, the completion of the crystallization route, and the immediate formation of pure materials. The DTG curve (**Figure 8**) demonstrates that at 86 °C, the maximum rate of decomposition of absorbed water molecules is around 0.37 mg/min. Exothermic and endothermic reactions are generally observed in the produced materials, as indicated by the DTA curve. According to the DTA curve (**Figure 8**), endothermic peaks are found at 86 °C as a result of dehydration and at 324 and 618 °C as a result of the decomposition of anhydrous precursor (Catalano & Di Benedetto, 2017).

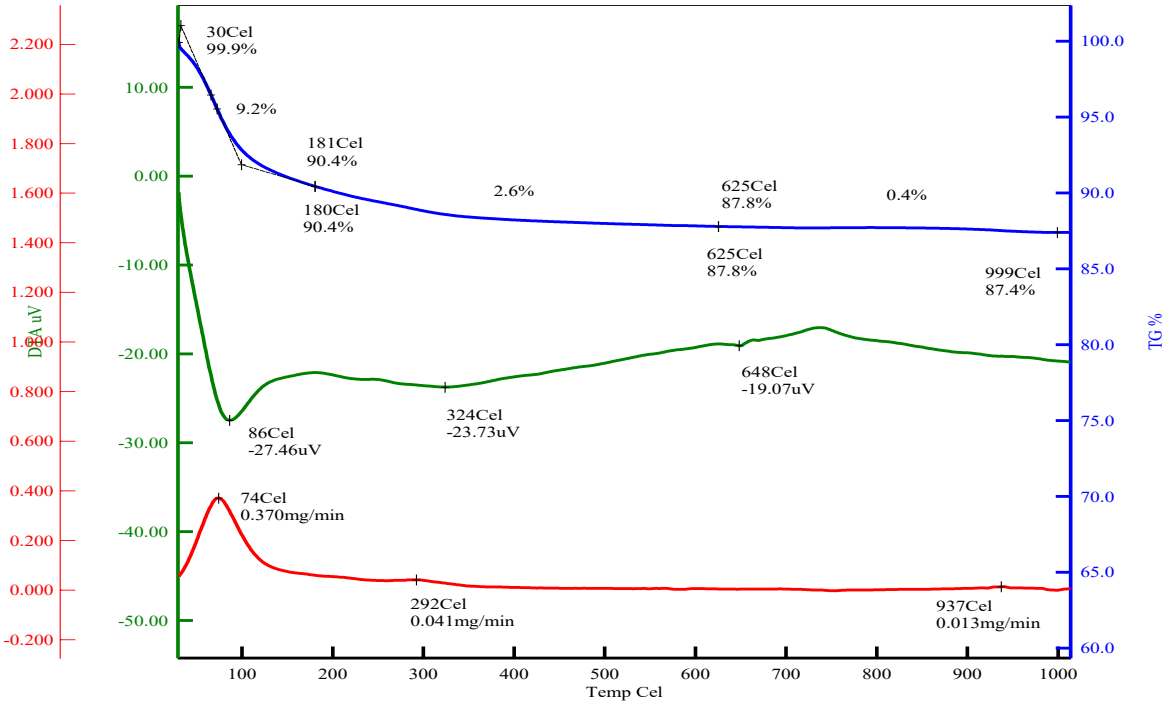

Figure 8. TG-DTA curve of Fe_3O_4 nanoparticles

3.8. UV-VIS Analysis

3.8.1. Degradation of Methyl Orange by Fe_3O_4 Nanoparticles:

Using Fe_3O_4 nanoparticles, the rate of degradation of MO is measured. The absorbance vs wavelength as well as absorbance vs time curves of MO with Fe_3O_4 NPs are shown in **Figures 9(a)**, and **9(b)**, respectively where it is seen that the absorbance peak of MO comes at 464 nm (Nandini & Vishalakshi, 2012). As seen in **Figure 9(c)**, the rate of degradation of MO grows progressively over time, reaching

its maximum after 60 minutes. As illustrated in **Figure 9(c),** the results demonstrate that the maximum rate of degradation of MO by Fe_3O_4 nanoparticles is 75.39%. According to a previous report, iron oxide nanoparticles can remove up to 73.6% of the color of MO dye (Kouhbanani *et al.,* 2019). In other publications, dyes such as MB, bromocresol green (BCG), and crystal violet (CV) were eliminated using iron oxide nanoparticles (Badeenezhad *et al.,* 2019; Nassar *et al.,* 2015). The kinetic plot of MO is shown in **Figure 9(d)** which indicates that the degradation of MO using Fe_3O_4 nanoparticles follows first-order kinetic. Because iron nanoparticles operate as reductants and catalysts to eliminate pollutants including lead, chromium, arsenic, and chlorinated solvents, they have a favorable effect on the environment (Aragaw *et al.,* 2021).

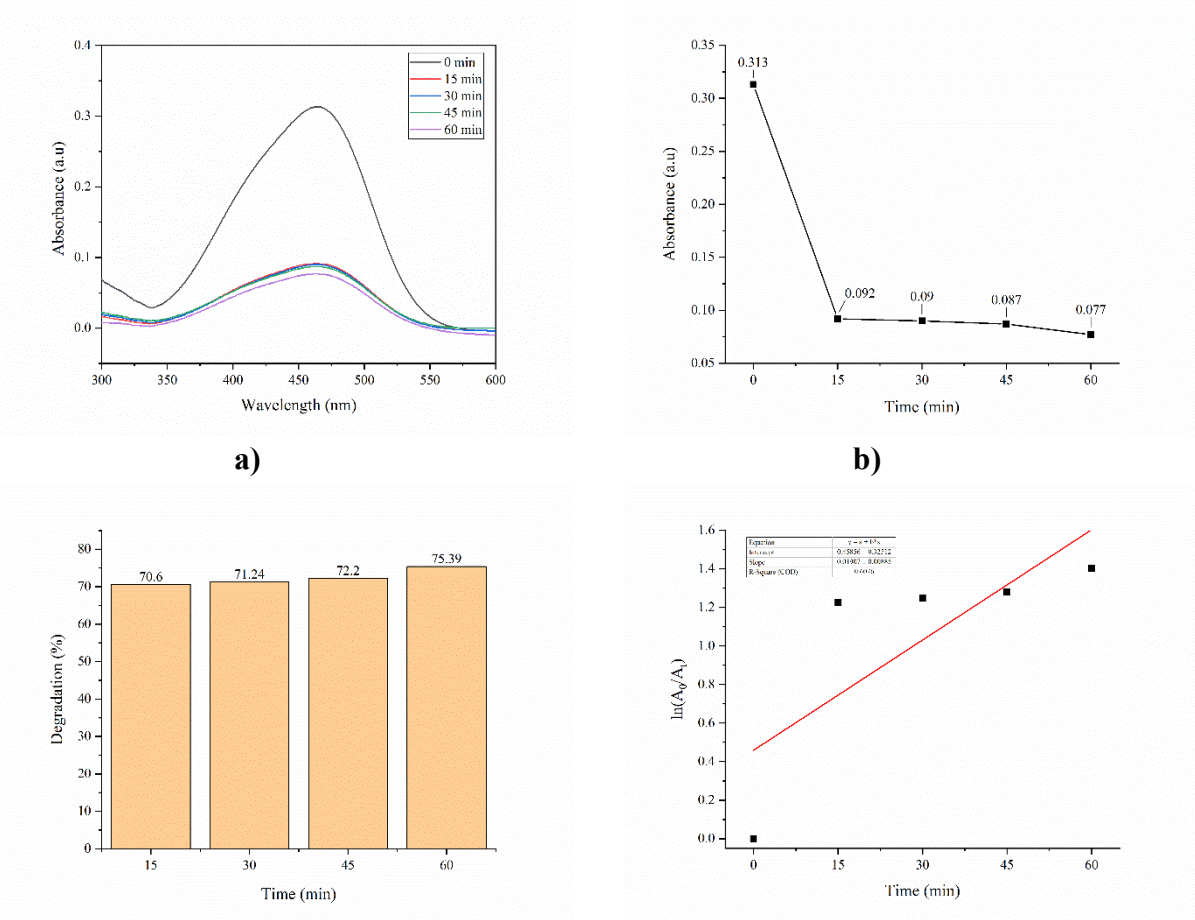

Figure 9. a) Absorbance vs wavelength curves of MO at different time intervals **b)** Absorbance vs time curve of MO **c)** Degradation of MO by Fe_3O_4 nanoparticles at different time intervals **d)** The kinetic plot of MO

3.8.2. Degradation of Sulfamethoxazole by Fe_3O_4 Nanoparticles:

Pharmaceutical contaminants known as SMX have drawn a lot of attention as a result of the reliance of people on drugs like antibiotics. These antibiotics have entered water streams through excretion and urine feces. Because of this, the concentrations are rising out of control, necessitating the employment

of more modern materials and practical techniques. The impact of Fe_3O_4 nanoparticles with time on SMX degradation was examined in this study. The absorbance vs wavelength as well as absorbance vs time curves of SMX with Fe_3O_4 NPs are shown in **Figures 10(a),** and **10(b),** respectively where it is seen that the absorbance peak of SMX comes at 265.50 nm (Stojković *et al.,* 2016). It should be mentioned that the degrading effect is observed every 30 minutes for 120 minutes. After 120 minutes, a maximum deterioration of 24.73% is attained (**Figure 10(c)**). These findings further show that, as shown in **Figure 10(d)** the degradation of SMX by Fe_3O_4 nanoparticles follows first-order kinetics. In our study, we saw a lower degradation rate of SMX than the expected value, and low degradation of 40% was obtained when iron oxide was degraded against tetracycline, another antibiotic (Olusegun *et al.,* 2021). They observed that the ability of antibiotics to degrade by photodegradation may be compromised if there is significant adsorption occurring between the catalyst surface and the pollutant before breakdown. The screening may prevent light from penetrating, which would imply that the creation of excited electrons and holes may be restricted.

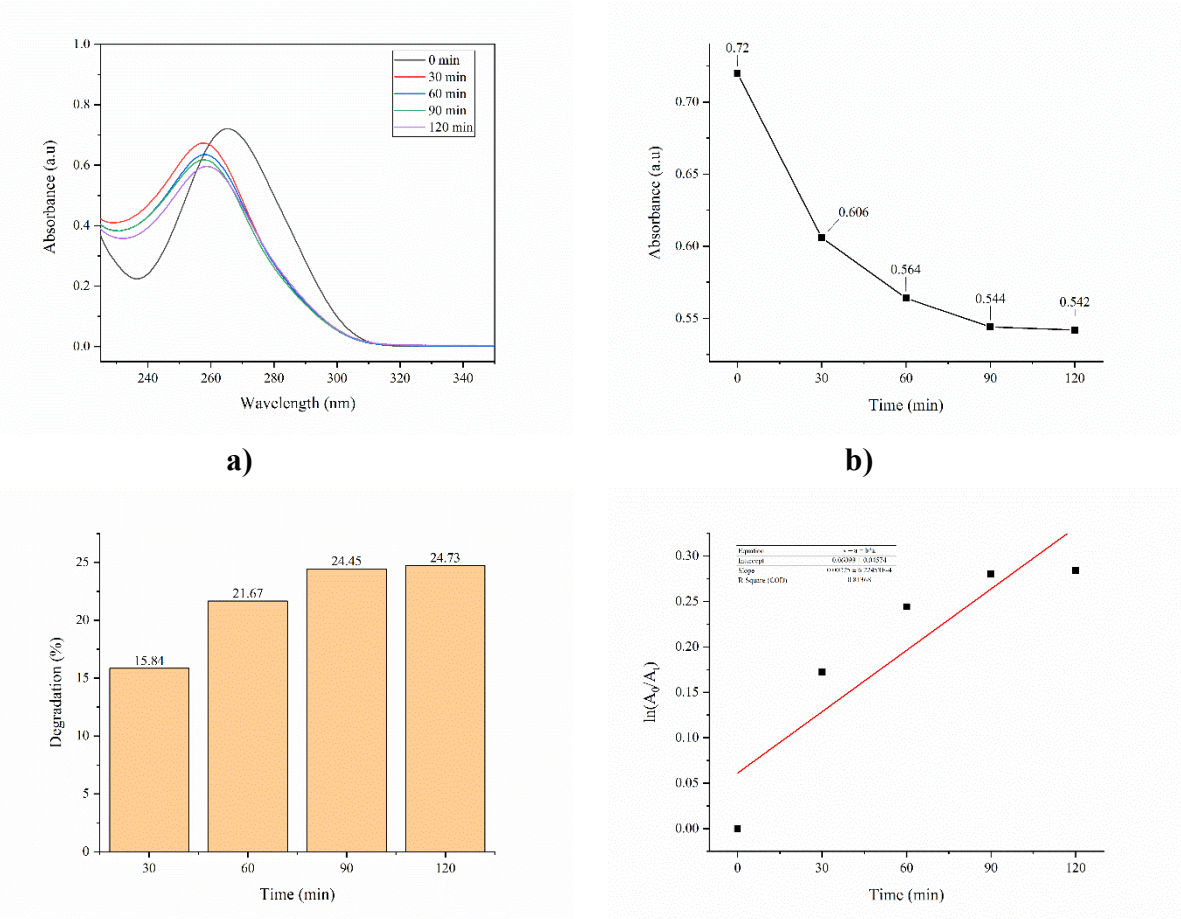

Figure 10. a) Absorbance vs wavelength curves of SMX at different time intervals **b)** Absorbance vs time curve of SMX **c)** Degradation of SMX by Fe_3O_4 nanoparticles at different time intervals **d)** The kinetic plot of SMX

Conclusion

Using iron salts as a precursor, an easy co-precipitation process in an aqueous solution was used to produce magnetite nanoparticles chemically. The produced magnetite nanoparticles had a spherical shape with an average diameter of about 30 nm, as shown by the TEM image. However, the AFM and SEM images indicate larger particle sizes because the particles agglomerated during the four hours of calcination at 250 °C. XRD data suggest that face-centered cubic magnetite could be the iron oxide crystal phase. Magnetization measurements as a function of the field revealed superparamagnetism behavior in the material since there was low coercitivity for the hysteresis cycles. The investigation into the degradation of organic dyes and antibiotics using superparamagnetic Fe_3O_4 nanoparticles synthesized through the chemical co-precipitation method has yielded valuable insights into the potential environmental applications of nanomaterials. The findings underscore the effectiveness of Fe_3O_4 nanoparticles as a promising catalyst for the degradation of pollutants, showcasing their ability to address challenges associated with water and wastewater treatment. The synthesis method employed in this research demonstrates a feasible and scalable approach for producing nanoparticles with enhanced catalytic properties. As we navigate environmental concerns and seek sustainable solutions, the outcomes of this study contribute significantly to the evolving field of nanotechnology and environmental science, opening avenues for further exploration and application of magnetic nanoparticles in pollution remediation strategies.

Acknowledgment

The authors appreciate the technical assistance provided by Pilot Plant and Process Development Center. Additionally, the technical assistance of Mr. Md. Shofiqul Islam and Mrs. Monira Binte Mesbah, Scientific Officers of Pilot Plant and Process Development Center are sincerely acknowledged by the authors.

Author Contributions

Md. Abdus Sabur was the major contributor and contributed to the conception of formulation, study designs, nanoparticle synthesis and characterization, data analysis, graphical design, figure illustrations, and manuscript writing. Md. Abdul Gafur was responsible for resources, supervision, and review. Md. Newaz Sharif was responsible for nanoparticle synthesis and characterization.

Funding Statement

The authors affirm that they did not accept any money, grants, or other assistance to create this manuscript.

Conflict-of-Interest Statement

The authors affirm that they have no known financial or interpersonal conflicts that would have appeared to impact the research presented in this study.

Data Availability Statement

Even though adequate data have been given in the form of tables and figures; however, all authors declare that if more data are required then the data will be provided on a request basis.

References

Aaddouz M., Azzaoui K., Akartasse N., Mejdoubi E., Hammouti B., Taleb M., Sabbahi R., Alshahateet S.F. (2023). Removal of Methylene Blue from aqueous solution by adsorption onto hydroxyapatite nanoparticles, *Journal of Molecular Structure,* 1288, 135807, https://doi.org/10.1016/j.molstruc.2023.135807

Abbas, M., Parvatheeswara Rao, B., Naga, S. M., Takahashi, M., Kim, C. (2013). Synthesis of high magnetization hydrophilic magnetite ($Fe3O_4$) nanoparticles in single reaction - Surfactantless polyol process. *Ceramics International*, 39(7), 7605–7611. https://doi.org/10.1016/j.ceramint.2013.03.015

Ahmed, M. J. K., Ahmaruzzaman, M., & Bordoloi, M. H. (2015). Novel Averrhoa carambola extract stabilized magnetite nanoparticles: A green synthesis route for the removal of chlorazol black e from wastewater. *RSC Advances*, *5*(91), 74645–74655. https://doi.org/10.1039/c5ra13970h

Akinola, P. O., Lateef, A., Asafa, T. B., Beukes, L. S., Hakeem, A. S., & Irshad, H. M. (2020). Multifunctional titanium dioxide nanoparticles biofabricated via phytosynthetic route using extracts of Cola nitida: antimicrobial, dye degradation, antioxidant and anticoagulant activities. *Heliyon*, *6*(8), e04610. https://doi.org/10.1016/j.heliyon.2020.e04610

Al-Hakkani, M. F., Gouda, G. A., & Hassan, S. H. A. (2021). A review of green methods for phyto-fabrication of hematite (α-Fe_2O3) nanoparticles and their characterization, properties, and applications. *Heliyon*, *7*(1), e05806. https://doi.org/10.1016/j.heliyon.2020.e05806

Alterary, S. S., & Alkhamees, A. (2021). Synthesis, surface modification, and characterization of Fe3O4@SiO2core@shell nanostructure. *Green Processing and Synthesis*, *10*(1), 384–391. https://doi.org/10.1515/gps-2021-0031

Anchan, S., Pai, S., Sridevi, H., Varadavenkatesan, T., Vinayagam, R., & Selvaraj, R. (2019). Biogenic synthesis of ferric oxide nanoparticles using the leaf extract of Peltophorum pterocarpum and their catalytic dye degradation potential. *Biocatalysis and Agricultural Biotechnology*, *20*, 101251. https://doi.org/10.1016/j.bcab.2019.101251

Andrade, M. B., Santos, T. R. T., Fernandes Silva, M., Vieira, M. F., Bergamasco, R., & Hamoudi, S. (2019). Graphene oxide impregnated with iron oxide nanoparticles for the removal of atrazine from the aqueous medium. *Separation Science and Technology (Philadelphia)*, *54*(16), 2653–2670. https://doi.org/10.1080/01496395.2018.1549077

Aragaw, T. A., Bogale, F. M., & Aragaw, B. A. (2021). Iron-based nanoparticles in wastewater treatment: A review on synthesis methods, applications, and removal mechanisms. *Journal of Saudi Chemical Society*, *25*(8), 101280. https://doi.org/10.1016/j.jscs.2021.101280

Arefi, M., Saberi, D., Karimi, M., Heydari, A. (2015). Superparamagnetic Fe(OH)3@Fe3O4 nanoparticles: An efficient and recoverable catalyst for tandem oxidative amidation of alcohols with amine hydrochloride salts. *ACS Combinatorial Science*, *17*(6), 341–347. https://doi.org/10.1021/co5001844

Azzaoui K., Aaddouz A., Akartase N., Mejdoubi E., Jodeh S., Hammouti B., Taleb M., Essehli S., Berisha A., Rhazi L., Lamhamdi A., Hanbali G., Algarra M., Dagdag O. (2024), Synthesis of β-Tricalcium phosphate/ PEG 6000 composite by novel dissolution/ precipitation method: Optimization of the Adsorption Process

using a Factorial Design: DFT and Molecular Dynamic, *Arabian Journal for Science and Engineering,* 49(1), 711-732, https://doi.org/10.1007/s13369-023-08390-8

Azzaoui K., Jodeh S., Mejdoubi E., Hammouti B., Taleb M., Ennabety G., Berisha A., Aaddouz M., Youssouf M.H., Shityakov S., Sabbahi R., Algarra M. (2023) Synthesis of hydroxyapatite /polyethylene glycol 6000 composites by novel dissolution/ precipitation method: Optimization of the Adsorption Process using a Factorial Design: DFT and Molecular Dynamic. *BCM Chemistry,* 17(1), 150. https://doi.org/10.1186/s13065-023-01061-7

Badeenezhad, A., Azhdarpoor, A., Bahrami, S., & Yousefinejad, S. (2019). Removal of methylene blue dye from aqueous solutions by natural clinoptilolite and clinoptilolite modified by iron oxide nanoparticles. *Molecular Simulation*, *45*(7), 564–571. https://doi.org/10.1080/08927022.2018.1564077

Bahadur, A., Saeed, A., Shoaib, M., Iqbal, S., Bashir, M. I., Waqas, M., Hussain, M. N., & Abbas, N. (2017). Eco-friendly synthesis of magnetite (Fe3O4) nanoparticles with tunable size: Dielectric, magnetic, thermal and optical studies. *Materials Chemistry and Physics*, *198*, 229–235. https://doi.org/10.1016/j.matchemphys.2017.05.061

Bhuiyan, M. S. H., Miah, M. Y., Paul, S. C., Aka, T. Das, Saha, O., Rahaman, M. M., Sharif, M. J. I., Habiba, O., & Ashaduzzaman, M. (2020). Green synthesis of iron oxide nanoparticle using Carica papaya leaf extract: application for photocatalytic degradation of remazol yellow RR dye and antibacterial activity. *Heliyon*, *6*(8), e04603. https://doi.org/10.1016/j.heliyon.2020.e04603

Bibi, I., Nazar, N., Ata, S., Sultan, M., Ali, A., Abbas, A., Jilani, K., Kamal, S., Sarim, F. M., Khan, M. I., Jalal, F., & Iqbal, M. (2019). Green synthesis of iron oxide nanoparticles using pomegranate seeds extract and photocatalytic activity evaluation for the degradation of textile dye. *Journal of Materials Research and Technology*, *8*(6), 6115–6124. https://doi.org/10.1016/j.jmrt.2019.10.006

Bødker, F., Mørup, S., & Linderoth, S. (1994). Surface effects in metallic iron nanoparticles. *Physical Review Letters*, *72*(2), 282–285. https://doi.org/10.1103/PhysRevLett.72.282

Bordbar, A. K., Rastegari, A. A., Amiri, R., Ranjbakhsh, E., Abbasi, M., & Khosropour, A. R. (2014). Characterization of Modified Magnetite Nanoparticles for Albumin Immobilization. *Biotechnology Research International*, *2014*, 1–6. https://doi.org/10.1155/2014/705068

Catalano, E., & Di Benedetto, A. (2017). Characterization of physicochemical and colloidal properties of hydrogel chitosan-coated iron-oxide nanoparticles for cancer therapy. *Journal of Physics: Conference Series*, *841*(1). https://doi.org/10.1088/1742-6596/841/1/012010

Chen, Y., Quan, X., Wang, Z., Lee, C., Wang, Z., Tao, P., Song, C., Wu, J., Shang, W., & Deng, T. (2016). Stably dispersed high-temperature Fe3O4/silicone-oil nanofluids for direct solar thermal energy harvesting. *Journal of Materials Chemistry A*, *4*(44), 17503–17511. https://doi.org/10.1039/c6ta07773k

Devi, H. S., Boda, M. A., Shah, M. A., Parveen, S., & Wani, A. H. (2019). Green synthesis of iron oxide nanoparticles using Platanus orientalis leaf extract for antifungal activity. *Green Processing and Synthesis*, *8*(1), 38–45. https://doi.org/10.1515/gps-2017-0145

Fernandes, D. M., Andrade, J. L., Lima, M. K., Silva, M. F., Andrade, L. H. C., Lima, S. M., Hechenleitner, A. A. W., & Pineda, E. A. G. (2013). Thermal and photochemical effects on the structure, morphology, thermal and optical properties of PVA/Ni0.04Zn0.96O and PVA/Fe 0.03Zn0.97O nanocomposite films. *Polymer Degradation and Stability*, *98*(9), 1862–1868. https://doi.org/10.1016/j.polymdegradstab.2013.05.003

Ganapathe, L.S.; Mohamed, M.A.; Mohamad Yunus, R.; Berhanuddin, D.D. (2020) Magnetite (Fe_3O_4) Nanoparticles in Biomedical Application: From Synthesis to Surface Functionalisation. *Magnetochemistry*, 6, 68; https://doi.org/10.3390/magnetochemistry6040068

González-González, R. B., Sharma, A., Parra-Saldívar, R., Ramirez-Mendoza, R. A., Bilal, M., & Iqbal, H. M. N. (2022). Decontamination of emerging pharmaceutical pollutants using carbon-dots as robust materials. *Journal of Hazardous Materials*, *423*(September 2021). https://doi.org/10.1016/j.jhazmat.2021.127145

Goya, G. F. (2002). Magnetic dynamics of Zn57Fe2O4 nanoparticles dispersed in a ZnO matrix. *IEEE Transactions on Magnetics*, *38*(5 I), 2610–2612. https://doi.org/10.1109/TMAG.2002.803204

Goya, G. F., Berquó, T. S., Fonseca, F. C., & Morales, M. P. (2003). Static and dynamic magnetic properties of spherical magnetite nanoparticles. *Journal of Applied Physics*, *94*(5), 3520–3528. https://doi.org/10.1063/1.1599959

Hufschmid, R., Arami, H., Ferguson, R. M., Gonzales, M., Teeman, E., Brush, L. N., Browning, N. D., & Krishnan, K. M. (2015). Synthesis of phase-pure and monodisperse iron oxide nanoparticles by thermal decomposition. *Nanoscale*, *7*(25), 11142–11154. https://doi.org/10.1039/c5nr01651g

Jandl, S., & Deslandes, J. (1981). Infrared spectra of HfS3. *Physical Review B*, *24*(2), 1040–1044. https://doi.org/10.1103/PhysRevB.24.1040

Jian, X., Wu, B., Wei, Y., Dou, S. X., Wang, X., He, W., & Mahmood, N. (2016). Facile Synthesis of Fe3O4/GCs Composites and Their Enhanced Microwave Absorption Properties. *ACS Applied Materials and Interfaces*, *8*(9), 6101–6109. https://doi.org/10.1021/acsami.6b00388

Juárez-Rojop, I. E., Tovilla-Zárate, C. A., Aguilar-Domínguez, D. E., Fuente, L. F. R. de la, Lobato-García, C. E., Blé-Castillo, J. L., López-Meraz, L., Díaz-Zagoya, J. C., & Bermúdez-Ocaña, D. Y. (2014). Phytochemical screening and hypoglycemic activity of carica papaya leaf in streptozotocin-induced diabetic rats. *Revista Brasileira de Farmacognosia*, *24*(3), 341–347. https://doi.org/10.1016/j.bjp.2014.07.012

Kalantari, K., Ahmad, M. B., Masoumi, H. R. F., Shameli, K., Basri, M., & Khandanlou, R. (2014). Rapid adsorption of heavy metals by Fe3O4/talc nanocomposite and optimization study using response surface methodology. *International Journal of Molecular Sciences*, *15*(7), 12913–12927. https://doi.org/10.3390/ijms150712913

Kiwumulo, H. F., Muwonge, H., Ibingira, C., Lubwama, M., Kirabira, J. B., & Ssekitoleko, R. T. (2022). Green synthesis and characterization of iron-oxide nanoparticles using Moringa oleifera: a potential protocol for use in low and middle income countries. *BMC Research Notes*, *15*(1), 1–8. https://doi.org/10.1186/s13104-022-06039-7

Kouhbanani, M. A. J., Beheshtkhoo, N., Taghizadeh, S., Amani, A. M., & Alimardani, V. (2019). One-step green synthesis and characterization of iron oxide nanoparticles using aqueous leaf extract of Teucrium polium and their catalytic application in dye degradation. *Advances in Natural Sciences: Nanoscience and Nanotechnology*, 10(1), 015007. https://doi.org/10.1088/2043-6254/aafe74

Li, Q., Kartikowati, C. W., Horie, S., Ogi, T., Iwaki, T., Okuyama, K. (2017). Correlation between particle size/domain structure and magnetic properties of highly crystalline Fe3O4 nanoparticles. *Scientific Reports*, *7*(1), 1–4. https://doi.org/10.1038/s41598-017-09897-5

Lima-Tenório, M. K., Gómez Pineda, E. A., Ahmad, N. M., Fessi, H., & Elaissari, A. (2015). Magnetic nanoparticles: In vivo cancer diagnosis and therapy. *International Journal of Pharmaceutics*, *493*(1–2), 313–327. https://doi.org/10.1016/j.ijpharm.2015.07.059

Mahlaule-Glory, L. M., Mapetla, S., Makofane, A., Mathipa, M. M., & Hintsho-Mbita, N. C. (2022). Biosynthesis of iron oxide nanoparticles for the degradation of methylene blue dye, sulfisoxazole antibiotic and removal of bacteria from real water. *Heliyon*, *8*(9), e10536. https://doi.org/10.1016/j.heliyon.2022.e10536

Mahmed, N., Heczko, O., Söderberg, O., & Hannula, S. P. (2011). Room temperature synthesis of magnetite (Fe3-δO 4) nanoparticles by a simple reverse co-precipitation method. *IOP Conference Series: Materials Science and Engineering*, *18*(SYMPOSIUM 2A), 3–7. https://doi.org/10.1088/1757-899X/18/3/032020

Morales, M. P., Andres-Vergés, M., Veintemillas-Verdaguer, S., Montero, M. I., & Serna, C. J. (1999). Structural effects on the magnetic properties of γ-Fe2O3 nanoparticles. *Journal of Magnetism and Magnetic Materials*, *203*(1–3), 146–148. https://doi.org/10.1016/S0304-8853(99)00278-4

Nandini, R., & Vishalakshi, B. (2012). A study of interaction of methyl orange with some polycations. *E-Journal of Chemistry*, *9*(1), 1–14. https://doi.org/10.1155/2012/343928

Nassar, N. N., Marei, N. N., Vitale, G., & Arar, L. A. (2015). Adsorptive removal of dyes from synthetic and real textile wastewater using magnetic iron oxide nanoparticles: Thermodynamic and mechanistic insights. *Canadian Journal of Chemical Engineering*, *93*(11), 1965–1974. https://doi.org/10.1002/cjce.22315

Olusegun, S. J., Larrea, G., Osial, M., Jackowska, K., & Krysinski, P. (2021). Photocatalytic degradation of antibiotics by superparamagnetic iron oxide nanoparticles. Tetracycline case. *Catalysts*, *11*(10). https://doi.org/10.3390/catal11101243

Prabhu, Y. T., Rao, K. V., Kumari, B. S., Kumar, V. S. S., & Pavani, T. (2015). Synthesis of Fe3O4 nanoparticles and its antibacterial application. *International Nano Letters*, *5*(2), 85–92. https://doi.org/10.1007/s40089-015-0141-z

Predoi, G., Ciobanu, C. S., Iconaru, S. L., Predoi, D., Dreghici, D. B., Groza, A., Barbuceanu, F., Cimpeanu, C., Badea, M. L., Barbuceanu, S. F., Furnaris, C. F., Belu, C., Ghegoiu, L., & Raita, M. S. (2021). Preparation and characterization of dextran coated iron oxide nanoparticles thin layers. *Polymers*, *13*(14). https://doi.org/10.3390/polym13142351

Rais Z., Taleb M., Sfaira M., Filali Baba M., Hammouti B., Maghnouj J., Nejjar R., Hadji M. (2008), Decolouration of textile's effluents discoloration by adsorption in static reactor and in dynamic reactor on the phosphocalcic apatites, *Phys. Chem. News,* 38, 106-111

Rezayan, A. H., Mosavi, M., Kheirjou, S., Amoabediny, G., Ardestani, M. S., & Mohammadnejad, J. (2016). Monodisperse magnetite (Fe3O4) nanoparticles modified with water soluble polymers for the diagnosis of breast cancer by MRI method. *Journal of Magnetism and Magnetic Materials*, *420*, 210–217. https://doi.org/10.1016/j.jmmm.2016.07.003

Sanaeifar, N., Rabiee, M., Abdolrahim, M., Tahriri, M., Vashaee, D., & Tayebi, L. (2017). A novel electrochemical biosensor based on Fe3O4 nanoparticles-polyvinyl alcohol composite for sensitive detection of glucose. *Analytical Biochemistry*, *519*, 19–26. https://doi.org/10.1016/j.ab.2016.12.006

Schwertmann, U. (2003). 14. Transformations. In *The Iron Oxides: Structure, Properties, Reactions, Ocurrences and Uses*.

Shaker Ardakani L., Alimardani V., Tamaddon A.M., Amani A.M., Taghizadeh S. (2021). Green synthesis of iron-based nanoparticles using Chlorophytum comosum leaf extract: methyl orange dye degradation and antimicrobial properties. *Heliyon*, 7(2), e06159. https://doi.org/10.1016/j.heliyon.2021.e06159

Stojković, G., Dimitrieska-Stojković, E., Soklevska, M., & Velev, R. (2016). Optimization, validation and application of UV-VIS spectrophotometric-colorimetric methods for determination of trimethoprim in different medicinal products. *Macedonian Veterinary Review*, *39*(1), 65–76. https://doi.org/10.1515/macvetrev-2015-0069

Thu Huong, L. T., Nam, N. H., Doan, D. H., My Nhung, H. T., Quang, B. T., Nam, P. H., Thong, P. Q., Phuc, N. X., & Thu, H. P. (2016). Folate attached, curcumin loaded Fe3O4 nanoparticles: A novel multifunctional drug delivery system for cancer treatment. *Materials Chemistry and Physics*, 172, 98–104. https://doi.org/10.1016/j.matchemphys.2015.12.065

Wang, B., Wei, Q., Qu, S. (2013). Synthesis and characterization of uniform and crystalline magnetite nanoparticles via oxidation-precipitation and modified co-precipitation methods. *International Journal of Electrochemical Science*, 8(3), 3786–3793. https://doi.org/10.1016/s1452-3981(23)14431-2

Wu, S., Sun, A., Zhai, F., Wang, J., Xu, W., Zhang, Q., Volinsky, A. A. (2011). Fe3O4 magnetic nanoparticles synthesis from tailings by ultrasonic chemical co-precipitation. *Materials Letters*, *65*(12), 1882–1884. https://doi.org/10.1016/j.matlet.2011.03.065

Wu, W., Jiang, C. Z., & Roy, V. A. L. (2016). Designed synthesis and surface engineering strategies of magnetic iron oxide nanoparticles for biomedical applications. *Nanoscale*, *8*(47), 19421–19474. https://doi.org/10.1039/c6nr07542h

(2024) ; http://www.jmaterenvironsci.com